

Organic-templating approach to synthesis of nanoporous silica composite membranes (I): TPA-templating and CO₂ separation

S. M. YANG*, Y. E. LEE*, S. H. HYUN*[§], C. H. LEE[‡]
 Departments of *Ceramic Engineering and [‡]Chemical Engineering,
 College of Engineering, Yonsei University, Seoul 120-749, Korea
 E-mail: prohsh@yonsei.ac.kr

Nanoporous silica composite membranes for gas separation have been synthesized by dip-coating the tetrapropylammonium (TPA)-templating silica sols on tubular alumina supports (pore size 2.8–100 nm), followed by eliminating the template via heat-treating at 550–600°C. The NMR spectroscopy of TPABr-silica hybrid composites obtained from the templated silica sols confirmed that TPA molecules (i.e., final pores) were uniformly distributed in the silica matrix. The average pore size and the specific surface area of an unsupported membrane prepared by firing the TPABr (6 wt%)-silica hybrid composite at 600°C were below 18 Å and 830 m²/g, respectively. Any defects such as cracks or pin-holes on the surface of amorphous silica composite membranes were not observed. The CO₂/N₂ separation factor of their composite membranes varied from 3.2 to 10.3 and their gas permeability from 10⁻⁸ to 10⁻⁹ mol/m² · s · Pa depending on the microstructure of aluminar supports. © 2002 Kluwer Academic Publishers

1. Introduction

Gas separation using ceramic membranes has evolved into a commercial technology for several industrially important gas separations such as CO₂/CH₄, CO₂/N₂, and O₂/N₂ in recent years. Specially, the separation/recovery process of CO₂ has been evaluated as a highly value-added process in point of view for prevention of environmental pollution such as the green-house effect. Membrane separation technology has been used extensively in various fields of separation processes because it is a simple and low energy method compared to other processes, such as extraction, distillation, adsorption, and cryogenic process [1]. In particular, ceramic composite membranes have higher thermal, chemical and regenerability than polymeric membranes, and thus are suitable for CO₂ separation efficiency.

Many researchers have tried to reduce the pore size of ceramic membranes to less than 10 Å and also to modify their surfaces in order to enhance the CO₂/N₂ separation factor by gas transport mechanisms such as molecular sieving, activated diffusion, and surface diffusion instead of using Knudsen diffusion. Many studies on the synthesis of micro-porous ceramic membranes have been investigated recently [2–5]. In particular, a number of attempts have been made to prepare zeolite membranes, because of their very small and uniform pore structures and their strong hydrophobicity which is expected to prevent the decline in gas permeability due to moisture adsorption [6, 7]. Research on the synthesis of a ZSM-5 zeolite membrane using a hydrother-

mal treatment has also been carried out in our laboratory, and the ZSM-5 composite membrane synthesized was shown to be highly effective for CO₂ separation [1]. Despite considerable advances in synthetic procedures, the challenge of synthesizing continuous, defect free, submicron thickness zeolite membranes to be met. In recent years, however, organic template-derived amorphous/nanoporous silica composite membranes with uniform pore sizes comparable to those in zeolites have been getting more attention [8, 9]. Such membranes are expected to exhibit highly molecular sieving behavior and high permeances, but their performances are not proven yet.

In this study, the nanoporous/amorphous silica composite membranes have been synthesized by sol-gel processing of silica sols templated with noncovalently bonded TPABr. The CO₂ separation efficiency of synthetic silica membranes has been examined through testing both the gas permeabilities of various gases and the separation factors of CO₂ to N₂ in their mixtures. The effects of templating process parameters on the microstructure and the CO₂ separation of the TPA-templated silica membranes are also discussed.

2. Experimental procedure

2.1. Preparation of TPA-Templating Silica Sols

The organic templating silica sols were prepared by mixing silica sols and the organic template (TPABr,

[§]Author to whom all correspondence should be addressed.

3–9 wt%) at room temperature and then aged at 50°C for 4–24 h. Silica sols were prepared from tetraethoxysilane (TEOS) using a two-step acid catalyzed procedure described in detail by the literature [10]. A final molar ratio of the silica sol equal to TEOS : EtOH : H₂O : HCl of 1.0 : 3.8 : 5.0 : 0.0053. The silica-template hybrid composite were prepared by evaporating organic templating silica sols in polystyrene dishes, and the unsupported membranes were prepared by heating silica gels at 200–700°C (heating rate, 1°C/min, holding time 2 h).

The degree of uniform dispersion of template in the silica matrix was evaluated by the NMR spectroscopy of TPABr-silica hybrid composites, and their thermal behavior was examined by TG/DTA. A specific area of the unsupported membranes was analyzed by Brunauer-Emmett-Teller (BET), and the microstructure of unsupported membranes was examined by SEM and EDS.

2.2. Synthesis and characterization of SiO₂ composite membranes

γ -Al₂O₃/ α -Al₂O₃ composite supports were prepared by a dip-coating of boehmite sols on tubular α -Al₂O₃ supports (8 mm outside diameter, 0.8 mm thickness 100 mm length, and 0.1 μ m mean pore diameter). The average pore size of the γ -Al₂O₃ layer was 2.8 nm. The preparation methods of the supports, the boehmite sols and the γ -Al₂O₃/ α -Al₂O₃ composite supports are given in detail in the literature [11–13]. The organic template-dried silica composite membranes were prepared by a dip-coating of the templating sols on the γ -Al₂O₃/ α -Al₂O₃ composite supports at room temperature followed by heating to 550°C at a heating rate of 1°C/min, holding for 2 h.

The microstructure of the nanoporous silica membranes was observed by SEM. The CO₂/N₂ permselectivity (ratio of CO₂ permeability to N₂ permeability) and the separation factors, $Y_{CO_2}(1 - X_{CO_2})/X_{CO_2}(1 - Y_{CO_2})$, were also determined by the same apparatus and method as before in our laboratory [1, 14].

3. Results and discussion

3.1. TPABr-silica hybrid composites

The organic ligands must be uniformly incorporated in the inorganic matrix. In this study, the degree of uniform dispersion of TPABr was examined by the ¹H-²⁹Si cross-polarization (CP) nuclear magnetic resonance (NMR) method. In general, the energy of ¹H-spin is larger than that of ²⁹Si-spin. Therefore if cross-polarization is generated, the energy of ¹H-spin is transferred to ²⁹Si-spin. The energy transferred from ¹H to ²⁹Si is proportional to $1/r^3$ (r : ¹H-²⁹Si molecular distances), and then the amplified energy of the ²⁹Si determines the template efficiency indirectly. Fig. 1 shows the NMR spectrum of the TPABr (6 wt%)-silica hybrid composites. As seen in Fig. 1, when cross-polarization is generated, the peak of ²⁹Si-spin is considerably amplified. This result indicates that the uniform templating in the silica matrix has been performed efficiently. The TG/DTA data of the TPABr-silica hybrid composites are given in Fig. 2. Up to about 250°C, shrinkage is pro-

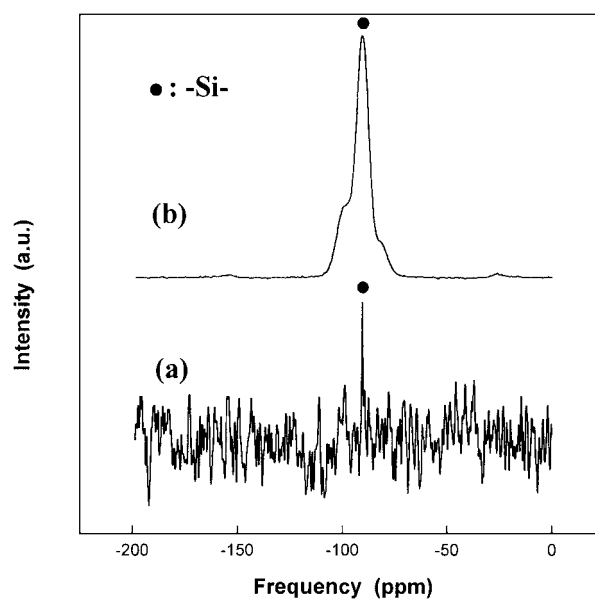


Figure 1 ¹H-²⁹Si cross-polarization (CP) NMR spectra of TPABr (6 wt%)-templating silica gel: (a) No CP and (b) CP.

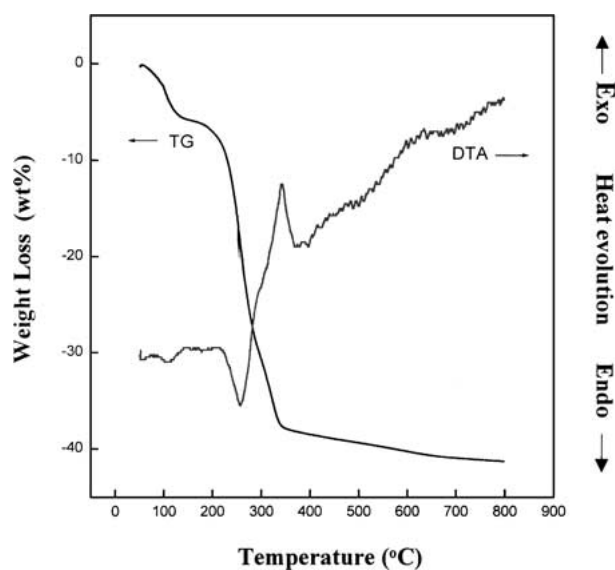


Figure 2 TG/DTA curves of the unsupported silica membrane prepared by TPABr-templating.

portional to weight loss suggesting that densification reactions expel water from the gel network. The sharp weight loss occurring between about 250–600°C is primarily attributed to the oxidative pyrolysis of TPABr and residual ethoxy ligand.

3.2. Unsupported silica membranes

Since it is very difficult to evaluate the characteristics of a membrane layer separately in the composite membranes, the characterization of the unsupported membranes must be done prior to preparing the composite membranes. Fig. 3 shows that the specific surface area variation of unsupported membranes with the heat treatment temperature and the amount of TPABr. The specific surface area of the unsupported membranes increased up to 400°C. A decreasing in the surface area from between about 400 to 700°C accounts for

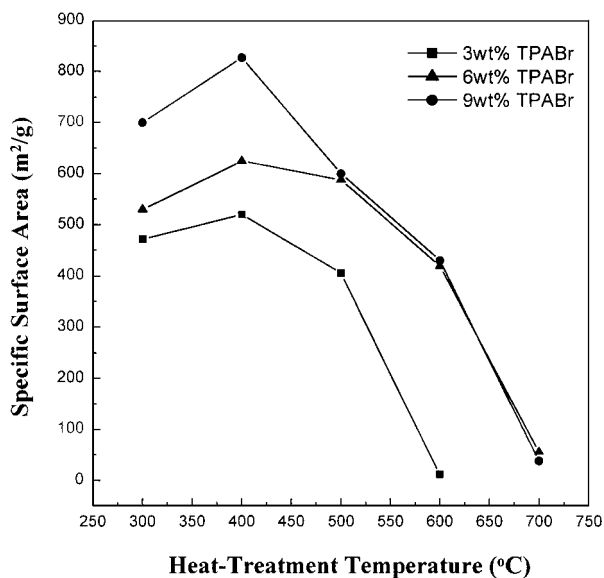


Figure 3 BET specific surface area versus heat-treatment temperature for unsupported silica membranes prepared by TPABr-templating.

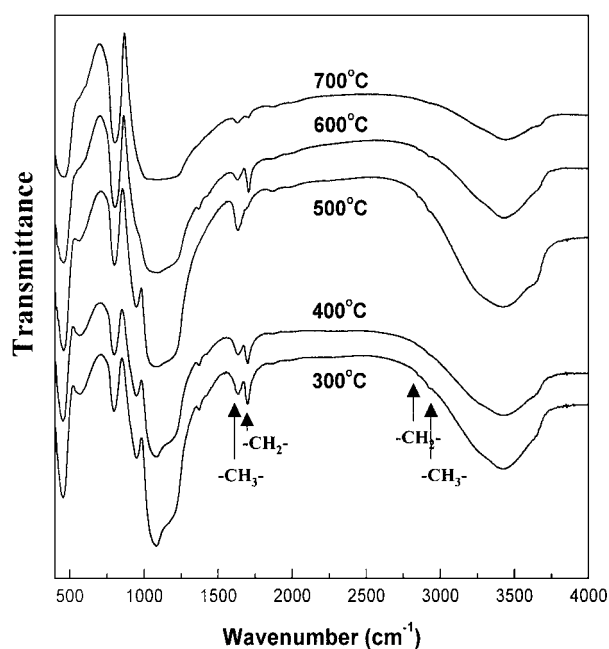


Figure 4 FT-IR spectra of unsupported silica membranes prepared by TPABr (6 wt%)-templating.

the densification of the SiO₂ network. The pore size of unsupported membrane was smaller than 18 Å. The decomposition temperature of TPABr is analyzed by the FT-IR (Fig. 4). The -CH₂- and -CH₃- of TPABr are removed completely above 600°C as can be seen in Fig. 4. This result agrees with the EDS data of Fig. 5. Fig. 5a shows a peak of Br, N and C, on the other hand Fig. 5b doesn't show any peak in the TPABr components. This result indicates that TPABr completely decomposes around 600°C.

3.3. Nanoporous silica composite membranes

Sol aging refers to the storage of the sol normally in a quiescent state under conditions appropriate to further

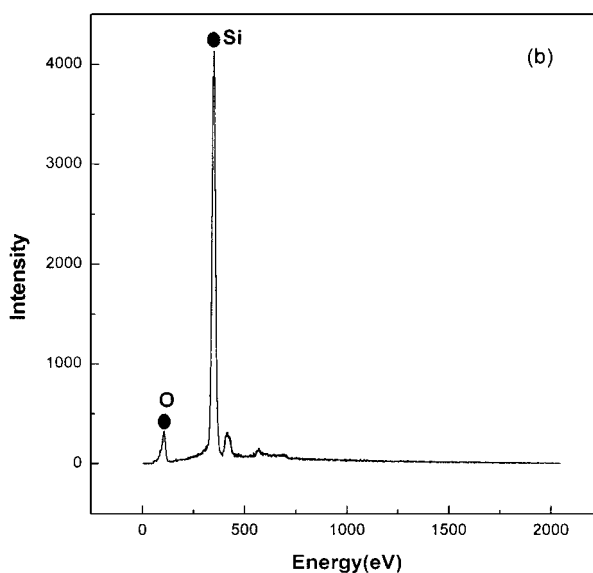
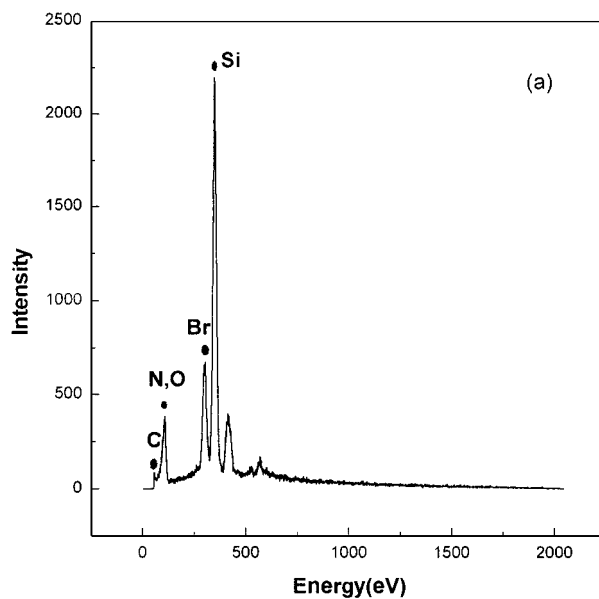


Figure 5 EDS data of unsupported silica membranes: (a) dried at room temperature and (b) heat-treated at 600°C.

the extents of hydrolysis, condensation, and/or ripening [13]. In accordance with the process of sol preparation, aging is used prior to gelation to grow polymeric species such that polymers are captured on top of the support with minimum pore penetration. Aging of sol is also used in organic (TPABr) and inorganic (silica) systems to uniformly incorporate organic ligands without aggregation of the organic and inorganic phases. For the sol clusters characterized by a mass fractal dimension, sol aging can be optimized to make the polymer species mutually transparent, so that they will interpenetrate during deposition and drying. Thus, aging can promote the densification of the network during deposition and drying, thereby creating very small pores and very narrow pore size distributions in gels and membranes.

The effect of aging on characteristics is illustrated in Table I. In the case of the γ -Al₂O₃/ α -Al₂O₃ composite support, the uniformity of the coating layer was not good, when aging time is for the range of about 12–24 h. This result means that sol is larger than the pore size of the γ -Al₂O₃/ α -Al₂O₃ composite support (2.8 nm)

TABLE I Coating characteristics of silica sols on γ -Al₂O₃/ α -Al₂O₃ composite supports depending upon aging time

Sol type (Aging time (h)/dilution ratio/coating time (s))	0/2/90	6/2/90	12/2/90	18/2/90	24/2/90
Sol particle size (nm)	<10 nm	<10 nm	<10 nm	<24 nm	<45 nm
Uniformity of coating layer	Excellent	Excellent	Good	Poor	Poor
After 1st-coating	2.26	0.713	0.692	–	–
N ₂ permeability $\times 10^7$ (mol/m ² · s · Pa)					

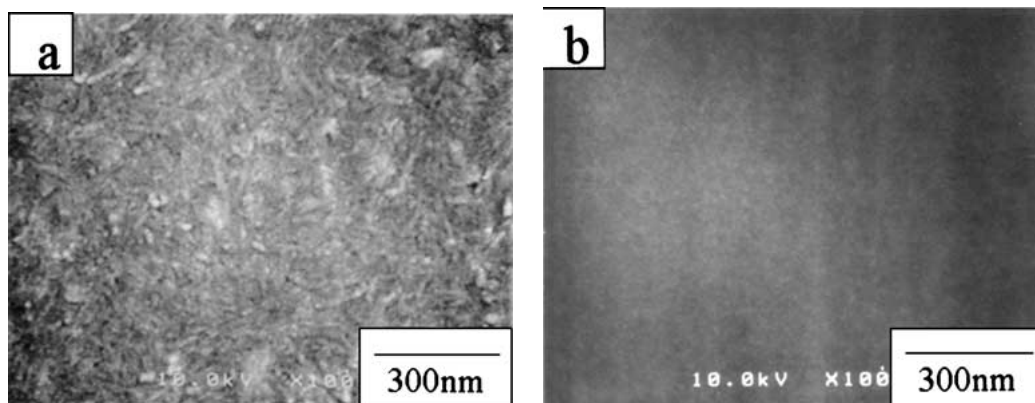


Figure 6 SEM micrographs of the SiO₂/ γ -Al₂O₃/ α -Al₂O₃ composite membrane prepared by dip-coating: (a) inner surface γ -Al₂O₃/ α -Al₂O₃ composite support before coating, (b) inner surface after coating.

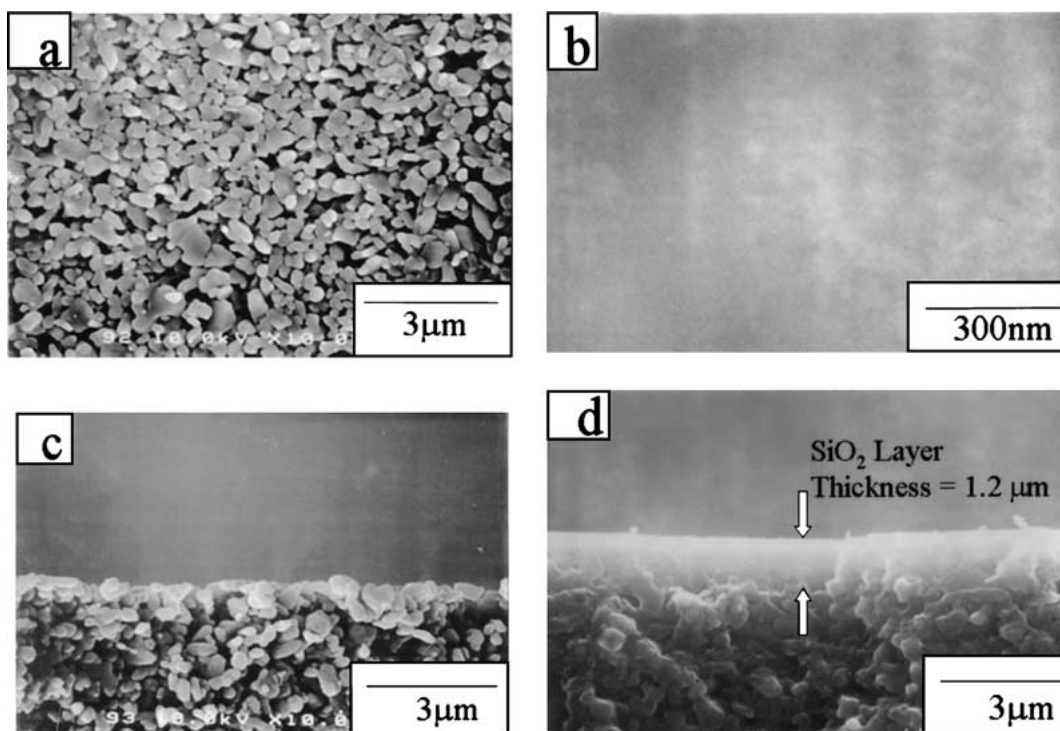


Figure 7 SEM micrographs of the SiO₂/ α -Al₂O₃ composite membrane prepared by the dip-coating: (a) inner surface of α -Al₂O₃ support, (b) inner surface of α -Al₂O₃/SiO₂ composite membrane, (c) inner fracture of α -Al₂O₃ support, and (d) inter fracture of α -Al₂O₃/SiO₂ composite membrane.

when the aging time of the sol is over 12 h. In the case of α -Al₂O₃ supports, however, this phenomenon was not observed. The microstructure of the SiO₂/ γ -Al₂O₃/ α -Al₂O₃ composite membrane is shown in Fig. 6. There are no crack on the surface of the SiO₂ layer, and the uniformity of the surface morphology is excellent. Be-

cause the sol concentration is low and particle size is too small (6 h aging) in comparison with the average pore size of the support to form a top layer, most of the sol particle is pore-filled coated. The penetration depth of the sol is about 5 μ m. Fig. 7 is the SEM picture of the SiO₂/ α -Al₂O₃ composite membrane. The SiO₂

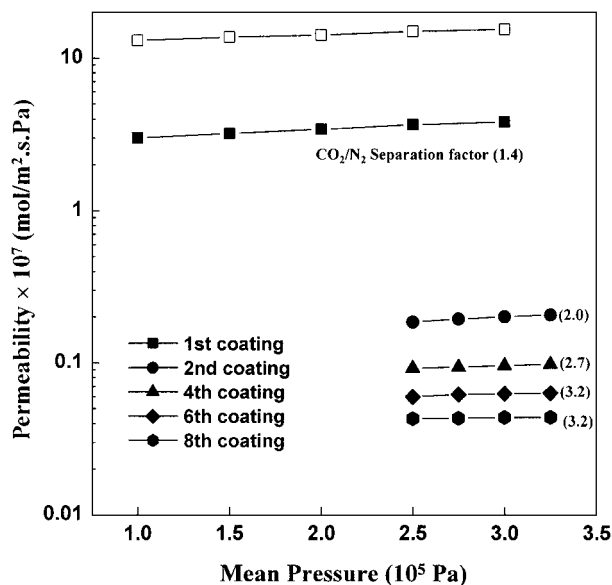


Figure 8 N_2 permeabilities of the $SiO_2/\gamma-Al_2O_3/\alpha-Al_2O_3$ composite membrane.

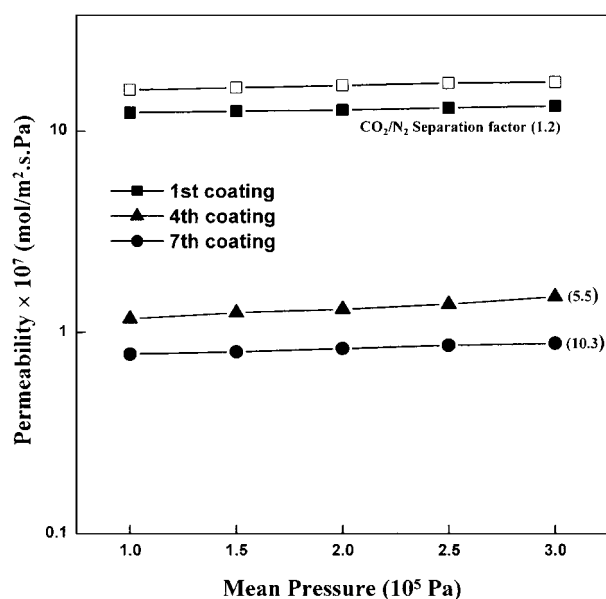


Figure 9 N_2 permeabilities of the $SiO_2/\alpha-Al_2O_3$ composite membrane.

top layer was formed on the $\alpha-Al_2O_3$ support. It was founded that the formation of the silica top layer were strongly dependent on the aging time of the sol and the pore size of the support. The differences in aging time have an effect on CO_2/N_2 separation factors. The separation factor of the $SiO_2/\gamma-Al_2O_3/\alpha-Al_2O_3$ using a sol aged for 6 h was 3.2, and that of $SiO_2/\alpha-Al_2O_3$ using a sol aged for 24 h was 10.3. This results may mean that the aging time determines the degree of densification of the SiO_2 films.

3.4. CO_2/N_2 Separation efficiency

3.4.1. Gas permeability

To minimize cracks or pin-holes in the silica layer, multi-coating was performed and the influence of the number of coating times on N_2 permeabilities of $SiO_2/\gamma-Al_2O_3/\alpha-Al_2O_3$ and $SiO_2/\alpha-Al_2O_3$ composite

membranes at room temperature is given in Figs 8 and 9, respectively. Since the thickness of the coating layer increases and the defects in the coating layer heal, the N_2 permeabilities decrease as the coating time increases. The N_2 permeabilities for the $SiO_2/\gamma-Al_2O_3/\alpha-Al_2O_3$ composite membrane are larger than those for the $SiO_2/\alpha-Al_2O_3$ composite membrane. This is caused by the fact that a $\gamma-Al_2O_3$ layer of $0.6 \mu m$ has already been formed in the $SiO_2/\gamma-Al_2O_3/\alpha-Al_2O_3$ composite membrane i.e. thickness of the membrane is larger than that of $SiO_2/\alpha-Al_2O_3$ composite membrane.

The $SiO_2/\alpha-Al_2O_3$ composite membrane was further evaluated by CO_2/N_2 , He/N_2 , He/Ar permselectivity and CO_2/N_2 separation factor measurement at $25^\circ C$. The gas permselectivities for the $SiO_2/\alpha-Al_2O_3$ composite membrane are given in Table II. As seen in Table II, CO_2/N_2 permselectivities for the $SiO_2/\alpha-Al_2O_3$ composite membrane increased considerably compared with the $\gamma-Al_2O_3/\alpha-Al_2O_3$ composite and the $\alpha-Al_2O_3$ supports. Also, while the CO_2/N_2 permselectivities for the $\gamma-Al_2O_3/\alpha-Al_2O_3$ composite and the $\alpha-Al_2O_3$ supports is almost same with CO_2/N_2 Knudsen ideal separation factor, CO_2/N_2 permselectivities for the $SiO_2/\alpha-Al_2O_3$ composite membrane is very higher than that. This means that synthesized $SiO_2/\alpha-Al_2O_3$ composite membrane has pores smaller than $20-50 \text{ \AA}$ (the region of Knudsen diffusion).

3.4.2. Separation factor of CO_2/N_2

The CO_2/N_2 separation factor of the $SiO_2/\gamma-Al_2O_3/\alpha-Al_2O_3$ composite membrane increased from 2.0 to 3.2 as the number of coating times increased from 2 to 6, but the separation factor did not increase considerably until around 5 times. For the $SiO_2/\alpha-Al_2O_3$ composite membrane, when the number of coating times was 4, the CO_2/N_2 separation factor was 5.5 and increased up to 10.3 (on the 7th coating).

To examine the effect of the separation process parameters on the CO_2/N_2 separation factor with transmembrane pressure, ΔP , and stage cut, θ , were measured. Fig. 10 shows the representative results of the effect of the transmembrane pressure for the $SiO_2/\alpha-Al_2O_3$ composite membrane. The CO_2/N_2 separation factor increased with the increase of the transmembrane pressure. This phenomenon can be explained by two mechanisms: (i) the CO_2 adsorption amount in the membrane pore could be increased with increasing pressure and (ii) back diffusion, caused by collision between gases having different molecular weights in gas mixtures, could be reduced by increasing the transmembrane pressure.

After faster permeation of CO_2 gas by preferential adsorption and surface diffusion, N_2 gas remains in the feed gas stream. Consequently, the concentration polarization phenomenon such as an increase in the N_2 concentration on the membrane surface, could appear. This can be reduced by flowing the feed gas with or without a sweep gas. In this work sweep gas was not used. The stage cut, i.e. the ratio of the permeate

TABLE II Permselectivities determined by the single gas permeation ratio of silica membrane layers at R.T

Membrane type	Single gas permeability $\times 10^7$ (mol/m ² · s · Pa)				Permselectivity		
	N ₂	CO ₂	He	Ar	CO ₂ /N ₂	He/N ₂	He/Ar
α -Al ₂ O ₃	15.592	13.029	38.164	12.866	0.84	2.45	2.97
γ -Al ₂ O ₃	13.143	11.184	33.491	10.525	0.85 (S.F: 1.2)	2.54	3.18
SiO ₂ / α -Al ₂ O ₃	0.013	0.034	0.024	0.01	2.62 (S.F: 10.3)	1.85	2.4

Ideal separation factor by Knudsen diffusion: CO₂/N₂ = 0.798, He/N₂ = 2.646, He/Ar = 3.16 S.F: Separation factor.

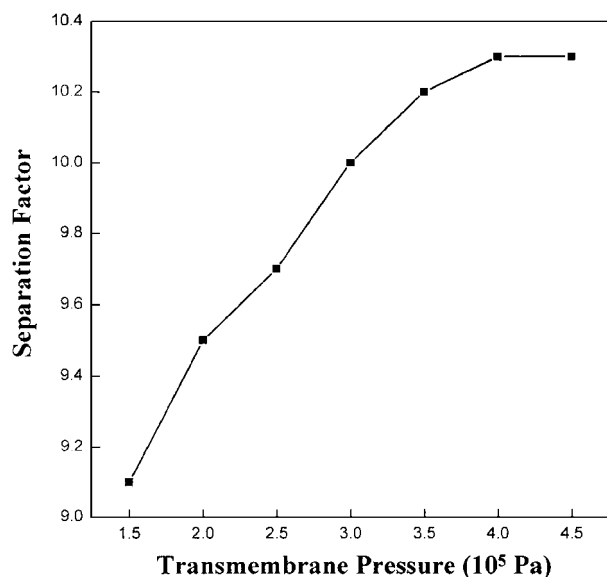


Figure 10 CO₂/N₂ separation factor versus transmembrane pressure of the SiO₂/ α -Al₂O₃ composite membrane.

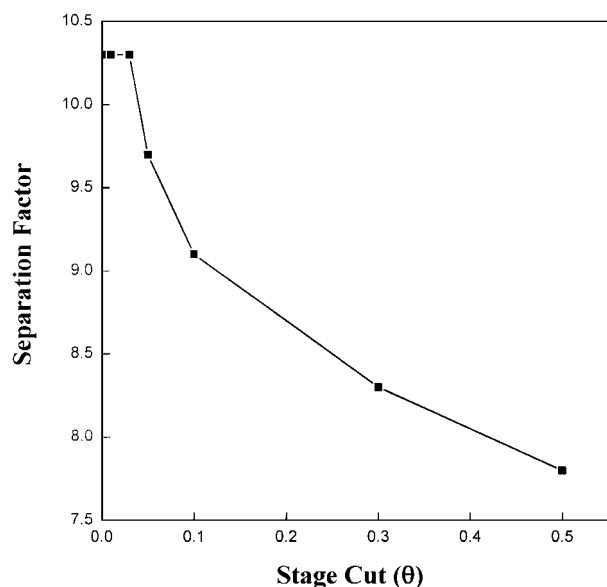


Figure 11 CO₂/N₂ separation factor versus stage cut (θ) for the SiO₂/ α -Al₂O₃ composite membrane.

flow rate to the retentate one, could then be a scale of the reduction of this concentration phenomenon. Variation of the CO₂/N₂ separation factor with stage cut is given for the SiO₂/ α -Al₂O₃ composite membrane as shown in Fig. 11. It can be clearly observed from Fig. 11 that the smaller the stage cut the higher the

CO₂/N₂. As stage cut is decreased from a scale of 0.5 to 0.03, the CO₂/N₂ separation factor increases from 7.8 to 10.3.

4. Conclusions

The amorphous/nanoporous silica composite membranes could be successively produced by an organic-templated approach. Porous α -alumina (pore size 100 nm) and γ -Al₂O₃/ α -Al₂O₃ (pore size 2.8 nm) tubes and TPA-templated silica sols were used as the membrane support and the coating sol, respectively. The main findings of this research are as follows.

1. TPA template-derived silica composite membranes without any defect could be prepared by dip-coating the silica sol with the mean particle size less than 10 nm on the γ -Al₂O₃/ α -Al₂O₃ support or larger than 40 nm on the α -Al₂O₃ support.

2. The uniform dispersion of the TPABr template in the silica matrix was confirmed by the ¹H-²⁹Si cross-polarization NMR spectroscopy for the TPABr-hybrid composite.

3. The average pore size and the specific surface area of an unsupported membrane prepared by firing the TPABr (6 wt%)-silica hybrid composite at 600°C were below 18 Å and about 830 m²/g, respectively.

4. The N₂ permeability and the CO₂/N₂ separation factor of the synthetic SiO₂/ γ -Al₂O₃/ α -Al₂O₃ composite membrane at room temperature was 3×10^{-9} mol/m² · s · Pa and 3.2, respectively, while those of the SiO₂/ α -Al₂O₃ composite membrane was 8×10^{-9} mol/m² · s · Pa and 10.3.

References

1. S. H. HYUN, J. K. SONG and B. I. KWAK, *J. Mater. Sci.* **34** (1999) 3095.
2. S. H. HYUN and B. S. KANG, *J. Amer. Ceram. Soc.* **77**(12) (1994) 3093.
3. *Idem.*, *ibid.* **79**(1) (1996) 279.
4. S. H. HYUN, S. C. YI and S. G. KIM, *J. Mater. Sci. Lett.* **15** (1996) 1384.
5. S. H. HYUN, S. Y. JO and B. S. KANG, *J. Membr. Sci.* **120** (1996) 197.
6. M. D. JIA, K. V. PEINEMAN and R. D. BEHLING, *ibid.* **82** (1993) 15.
7. Y. YAN, M. E. DAVIS and G. R. GAVALAS, *Ind. Eng. Chem. Res.* **34** (1995) 1652.
8. N. K. RAMAN, M. T. ANDERSON and C. J. BRINKER, *Chem. Mater.* **8** (1996) 1682.
9. N. K. RAMAN and C. J. BRINKER, *J. Membr. Sci.* **105** (1995) 273.

10. C. J. BRINKER and G. W. SCHERER, "Sol-Gel Science: The Physics and Chemistry of Sol Gel Processing" (Academic Press, San Diego, CA, 1990).
11. S. H. HYUN, S. Y. JO and B. S. KANG, *J. Membr. Sci.* **120** (1996) 197.
12. S. H. HYUN and B. S. KANG, *J. Amer. Ceram. Soc.* **79** (1994) 3093.
13. S. H. HYUN, B. S. KANG and D. J. CHOI, *J. Korean Ceram. Soc.* **29** (1992) 970.
14. B. S. KANG and S. H. HYUN, *J. Mater. Sci.* **34** (1999) 1393.
15. C. J. BRINKER and G. W. SCHERER, "Sol-Gel Science: The Physics and Chemistry of Sol-Gel Processing" (Academic Press, San Diego, CA, 1990) ch. 6.

*Received 23 April 2001
and accepted 14 February 2002*